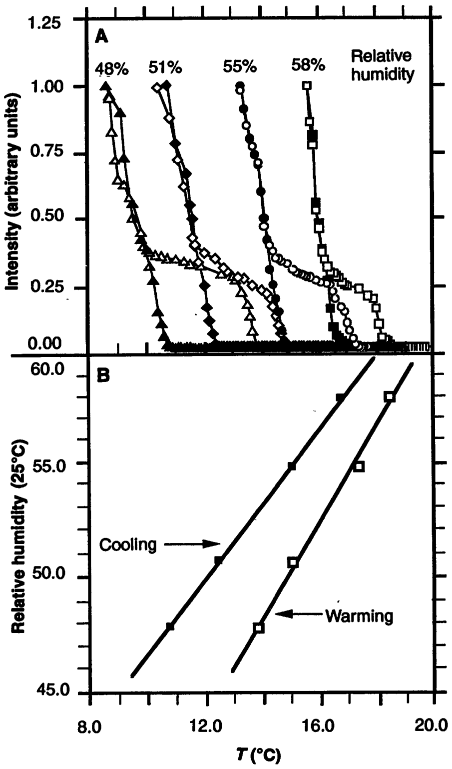

Fig. 4. (**A**) Plot of intensity of a first-order diffraction spot as a function of temperature *T* of the surface. Under atmospheres of different relative humidities, the surface shown in Fig. 3A was cooled or warmed, and the intensity of a first-order diffraction spot was monitored with a UDT-Silicon photodiode (United Detector Technologies, Irvine, California). The solid points were measured as the sample was cooled (0.5° to 1°C per second), and the open points were measured as the sample was warmed (1° to 2°C per second). (**B**) The intercepts on the *T* axis of lines fit to the rising and falling portions of the curves shown in (A) are linearly related to the relative humidity.

ple was cooled or warmed, and its temperature was monitored with a thermocouple. The quantitative change in intensity as a function of sample temperature for a first-order diffraction spot under atmospheres of different relative humidities is depicted in Fig. 4A (9). In all cases, as the temperature of the surface decreased, there was initially a slow rise in intensity (not visible in Fig. 4A), followed by a rapid rise. As the sample was cooled further, the water droplets began to bridge across the hydrophobic regions, and a decrease in intensity was observed (not shown). The warming curves exhibited significant hysteresis from the cooling curves. This hysteresis may be due to several factors. During cooling, the surface temperature must be low enough for nucleation of droplets to occur. During warming, the dewetting process is dependent on factors such as the local humidity near the surface and the surface-to-volume ratio of the drops as their size changes. In addition, advancing and receding contact angle measurements on surfaces of SAMs exhibit considerable hysteresis, reflecting the different factors that control wetting and dewetting (*10*).

Figure 4B shows linear relations between relative humidity (over the range from 48 to 58% at 25°C) and the intercept on the temperature axis for a line fit through the rapidly rising portion of the cooling curves and the rapidly decreasing portion of the warming curves. These data demonstrate that diffraction from these systems of patterned SAMs is very sensitive to relative humidity and suggest the use of these systems as sensors for humidity and other environmental factors. In addition to diffraction in a reflective geometry, these systems also produce diffraction in a transmission geometry. The use of semitransparent, thin (100 to 300 Å) gold films, deposited on glass slides (*11*), allowed diffraction from condensation figures to be observed for incident beams that were transmitted *through* the condensation figure.

These studies demonstrate the utility of regularly patterned SAMs as diffracting systems with which to analyze and use CFs. The ability to change the size, shape, and chemical composition of multiple arrays of spots simultaneously and independently, and to study the diffraction of light from them as a function of properties—the vapor pressure of condensable vapors, temperature, and concentrations of materials that might adsorb from solution or suspension—of the environment surrounding the surface that influence their reflectivity make these systems highly flexible tools with which to study phenomena in surface science (*12*). Their versatility, and the ability to use optical methods for assay, may provide advantages in designing sensors that are not practical with other techniques. In addition, this very sensitive method of characterizing CFs will be useful in studying the process of nucleation and formation and breakup of thin films.

REFERENCES AND NOTES

1. Lord Rayleigh, *Nature* **86**, 416 (1911); J. Aitken, *ibid.*, p. 516; Lord Rayleigh, *ibid.* **90**, 436 (1912); R. Merigoux, *Rev. Opt.* **9**, 281 (1937).
2. C. M. Knobler, *Physica A* **140**, 198 (1986); D. Beysens and C. M. Knobler, *Phys. Rev. Lett.* **57**, 1433 (1986); F. Perrot and D. Beysens, *Rev. Sci. Instrum.* **58**, 183 (1987); B. J. Briscoe and K. P. Galvin, *Colloids Surf.* **56**, 263 (1991).
3. G. P. López, H. A. Biebuyck, C. D. Frisbie, G. M. Whitesides, *Science* **260**, 647 (1993).
4. A. Kumar and G. M. Whitesides, *Appl. Phys. Lett.* **63**, 2002 (1993).
5. A. Kumar, H. A. Biebuyck, N. L. Abbott, G. M. Whitesides, *J. Am. Chem. Soc.* **119**, 4198 (1992).
6. N. L. Abbott, J. P. Folkers, G. M. Whitesides, *Science* **257**, 1380 (1992).
7. Although the data reported in the work was obtained from alkanethiolate SAMs supported on gold, similar results were obtained for SAMs on copper and silver.
8. G. P. López, H. A. Biebuyck, G. M. Whitesides, *Langmuir* **9**, 1513 (1993).
9. Relative humidity was measured with an analog hygrometer from Fisher Scientific (Pittsburgh, PA).
10. J. P. Folkers, P. E. Laibinis, G. M. Whitesides, *Langmuir* **8**, 1330 (1992).
11. P. A. DeMilla *et al.*, unpublished results.
12. A sensor based on diffraction from patterns of adsorbed proteins has been demonstrated; S. Deshpande and R. M. Rocco, Idetek Corporation, Sunnyvale, CA.
13. Supported in part by the Office of Naval Research, ARPA, and by the National Science Foundation (grant NSF PHY-9312572).

23 September 1993; accepted 8 November 1993

Fluorescent X-ray Interference from a Protein Monolayer

Yuji C. Sasaki,* Yoshio Suzuki, Tadashi Ishibashi

Fluorescent x-ray interference patterns have been observed from monolayers of both a metal-containing protein (ferritin) and a nonmetal-containing protein [bovine serum albumin (BSA)] bound on a gold substrate. These interference patterns have been used to determine structure data. The nonmetal-containing protein was first reacted with metal ions by means of a chelate compound to place the necessary chromophore in the molecule. The size of the ferritin core measured by a scanning electron microscope agrees with the value obtained from the x-ray interference experiments. In the BSA molecule, the measured interference fringe is consistent with the model in which the short axes of BSA molecules are perpendicular to the surface substrate.

As early as in 1934, Kossel (*1, 2*) observed the interference effects of characteristic x-rays within single crystals. Hutton *et al.* (*3*) discussed the phase information from the Kossel cone analysis of a perfect crystal. We have observed an interference pattern of fluorescent x-rays in noncrystalline media (*4*).

Fluorescent x-rays from a source atom above a substrate can take two optical paths

---

Advanced Research Laboratory, Hitachi Ltd., Hatoyama, Saitama, 350-03, Japan.

*To whom correspondence should be addressed.

(Fig. 1): direct emission and emission totally reflected from the substrate surface. Interference fringes can be clearly observed when the take-off angle (θ_t) for fluorescent x-rays is smaller than the critical angle (θ_c) for the total reflection of fluorescent x-rays because x-ray reflectivity is nearly 100%. The path difference between the two emissions is $2z \sin \theta_t$, where z is the distance of an emitting atom from the substrate. Thus, z may be determined from the oscillation period of interference fringes.

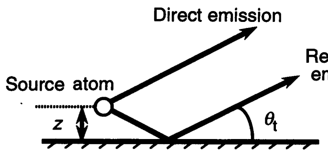

Fig. 1. Illustration of the principle of fluorescent x-ray interference between a direct and a totally reflected fluorescent emission; z is the distance between the substrate and the atom excited by the primary x-ray beam and θ_t is the take-off angle of fluorescent x-rays.

We applied this method to noncrystallized protein monolayer membranes containing labeling metal atoms. Our model samples are iron atoms in ferritin cores and zinc-labeled BSA molecules. Such experiments are a means of determining important structural information.

The nonmetal-containing protein, BSA (Sigma), was first reacted with the cyclic anhydride of diethylenetriaminepentaacetic acid (DTPA-anhydride) (5) and then labeled with zinc atoms. The ferritin (Sigma) and DTPA-BSA proteins were put on a polydiacetylene-coated (6) gold substrate by the Langmuir-Blodgett (LB) method. The protein molecules were electrostatically adsorbed in a monolayer form by the positively charged LB monolayer [1-docosylpyridinum bromide (DP)] at the air-water interface (Fig. 2). In our experimental setup (Fig. 3), the primary beam was fixed to the glancing angle (θ_g), where the total intensity of the fluorescent x-ray was maximum (4).

As seen in the fluorescent x-ray interference (FXI) pattern of iron Kα (Fig. 4A) from ferritin cores and zinc Kα (Fig. 4B) from the labeled BSA, there are two fringes below 14 mrad. In the theoretical FXI pattern, we modeled three homogeneous media—air, LB film containing the monolayer of the protein, and gold substrate—as stratified media (Fig. 2). The propagation of fluorescent x-rays in a stratified media (7) can be obtained on the basis of both reciprocity and the optical electromagnetic wave solution of Maxwell's equations on each interface. Thus, the angular distribution of the fluorescent x-rays can provide very precise information about the atomic

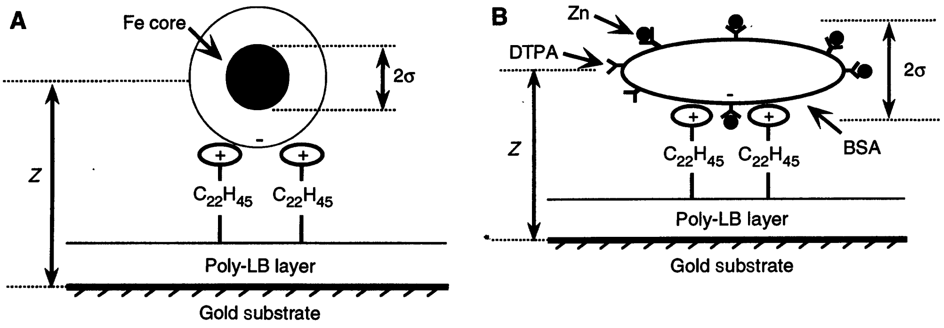

Fig. 2. Structure model of the protein monolayer. (**A**) Ferritin monolayer; (**B**) BSA monolayer, created by reaction with zinc-labeled DTPA-anhydride; z is the distance between the gold substrate and the position of the maximum peak in the distribution of the metal atoms, and 2σ is the distributed width for z. The DP solvent (0.5 mg per milliliter of chloroform) was spread on the surface of the subphase containing a 0.5 M acetate buffer at room temperature (pH 6.0). The proteins were suspended in the subphase and incubated at room temperature for about 1 hour. The protein-DP layer was transferred to the substrate at 20 to 25 mN/m by the horizontal dipping method. The gold substrate was coated with polydiacetylene (poly-dibutyl-4,17-dioxo-5,16-dioxa-3,18-diaza-9,11-eicosadiyne-dioate). Finally, the transferred protein LB film was rinsed with ultrapure water. The BSA protein was prepared as follows: 1 mg of DTPA-anhydride (Dojindo, Kumamoto, Japan) was added to 1 ml of BSA solution (20 mg per milliliter of 0.1 M Hepes buffer at pH 6.0). This solution (DTPA-BSA) was dialyzed overnight against a 0.5 M acetate buffer at 4°C. As a result of free amino groups determination (*12*) with 2,4,6-trinitrobenzen esulforic acid, 30 to 40% of the free amino groups in the BSA were labeled by DTPA-anhydride. A 1:1 mixture of the labeled BSA solution and $ZnCl_2$ solution (4.2 mg per milliliter of 0.5 M acetate buffer at pH 6.5) was dialyzed overnight against the 0.5 M acetate buffer (1 liter) at 4°C. The labeling of zinc atoms was confirmed by the inductively coupled plasma method to be 40 to 50%. Without the DTPA process, only a small percentage of the BSA molecules were labeled with zinc atoms.

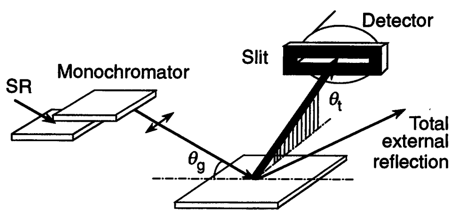

Fig. 3. Experimental apparatus for FXI measurement [BL-8C2 branch beam line in the National Laboratory for High Energy Physics (KEK) Photon Factory, 2.5-GeV storage ring]. The synchrotron radiation (SR) was linearly polarized in the horizontal plane and monochromated with a pair of Si (111) crystals passed through an ionization chamber. A slit 100 μm high and 6 mm wide was used to narrow the incident x-ray beam. Fluorescent radiation was measured perpendicular to the plane of the primary beam to minimize elastic background radiation. The angular distribution of the fluorescent x-rays was monitored with a pure-Ge detector (an energy dispersive detector) and with a slit (50 μm high and 12 mm wide, 200 mm from the sample) to determine θ_t. The angular resolution was less than 0.5 mrad in the measured region.

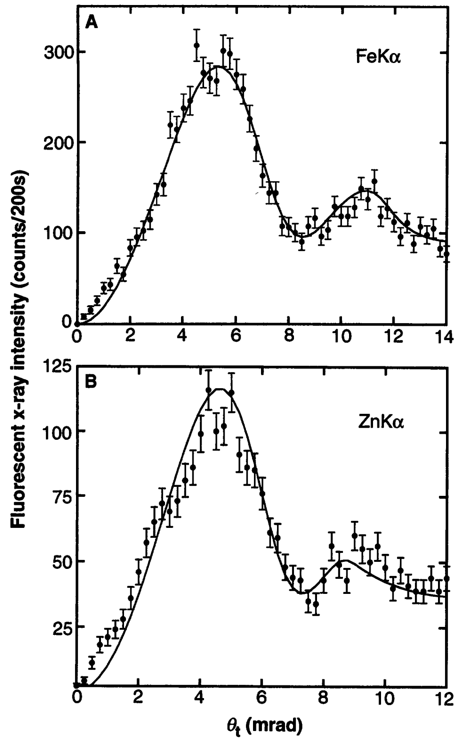

Fig. 4. (**A**) The iron Kα FXI pattern from the ferritin and (**B**) the zinc Kα FXI pattern from the DTPA-BSA. The amplitude of the calculated FXI pattern (solid line) was normalized to the intensity of the experimental FXI pattern (dots). The theoretical estimate for the normalized yield was calculated from the values of 1 − (the complex refractive indices), which are, for LB film and Au film, respectively, $(6.10 + 0.018\,i) \times 10^{-6}$ and $(6.86 + 0.600\,i) \times 10^{-5}$ for iron Kα, $(4.56 + 0.011\,i) \times 10^{-6}$ and $(5.13 + 0.396\,i) \times 10^{-5}$ for the ferritin experiment $\lambda_p = 1.67$ Å, $(4.89 + 0.010\,i) \times 10^{-6}$ and $(3.83 + 0.358\,i) \times 10^{-5}$ for zinc Kα, and $(3.89 + 0.009\,i) \times 10^{-6}$ and $(3.05 + 0.264\,i) \times 10^{-5}$ for the BSA experiment $\lambda_p = 1.28$ Å.

structure of surfaces and interfaces, for example, the value of z and the distributed width for z.

From the reciprocity theorem, the calculation of fluorescent x-ray intensity Y from coordinate z on the take-off angle θ_t is identical with that of incident x-ray field at coordinate z on the glancing angle θ_t. Thus, when atoms act as fluorescent x-ray sources with a distribution N, the yield Y should be

$$Y(\theta_t) = \int I(\theta_g, \lambda_p, z)\, N(z, \sigma)\, I(\theta_t, \lambda_f, z)\, dz \tag{1}$$

where $I(\theta_g, \lambda_p, z)$ is the primary x-ray intensity, which is affected by the total reflection beams for the incident wavelength λ_p at coordinate z. The distribution $N(z, \sigma)$ reaches a maximum at $z = z_0$ and is assumed to obey a Gaussian distribution with standard deviation σ (see Fig. 2). The intensity $I(\theta_t, \lambda_f, z)$ for fluorescent x-ray wavelength λ_f results from interference between the direct and totally reflected fluorescent emissions at coordinate z.

We obtained z_0 and the width 2σ for χ^2 minimization fit for $Y(\theta_t)$. The theoretical FXI pattern is in close agreement with the experimental one (Fig. 4). The values of the refractive indices of the gold substrate and of the LB film were obtained from the separate fitting of the x-ray reflectivities at the corresponding four wavelengths.

The fitted values and their 1σ confidence intervals for iron (Fig. 4A) are $z_0{}^{\mathrm{Fe}} = 95 \pm 14$ Å and $2\sigma^{\mathrm{Fe}} = 60\,^{+20}_{-14}$ Å. The size of the ferritin core (*8*), measured by a scanning electron microscope (Hitachi S-900), agrees with the $2\sigma^{\mathrm{Fe}}$ value obtained here. For BSA (Fig. 4B), $z_0{}^{\mathrm{Zn}} = 63\,^{+17}_{-31}$ Å and $2\sigma^{\mathrm{Zn}} = 58\,^{+26}_{-16}$ Å. The form of the BSA molecule, based on electron microscope observation with a metal coating (*9*), is a prolate ellipsoid with a major axis $2a = 140$ Å and a minor axis $2b = 40$ Å. Thus, our value of $2\sigma^{\mathrm{Zn}}$ is in close agreement with the value of the short axis for the BSA molecules. Consequently, the experimental FXI pattern is consistent with a model in which the short axes of BSA molecules are perpendicular to the surface of the substrate.

Information obtained from our FXI fringes is similar to that from x-ray standing waves generated by total reflection (*10*). However, FXI measurements have some advantages (*4*). Parallel and monochromatic x-rays are unnecessary because fluorescent radiation occurs independently of the primary beam (*11*). Thus, white x-ray beams of synchrotron radiation, electrons, and ions can be used as the primary beam. We hope that the FXI method can effectively measure conformational changes for noncrystallized proteins in wet conditions.

REFERENCES AND NOTES

1. W. Kossel, V. Loeck, H. Voges, *Z. Phys.* **94**, 139 (1935).
2. M. v. Laue, *Ann. Phys. Leipzig* **23**, 705 (1935).
3. J. T. Hutton, G. T. Trammell, J. P. Hannon, *Phys. Rev. B* **31**, 6420 (1985).
4. Y. C. Sasaki, Y. Suzuki, Y. Tomioka, A. Fukuhara, *ibid.* **48**, 7724 (1993).
5. D. J. Hnatowich, W. W. Layne, R. L. Childs, *Int. J. Appl. Radiat. Isot.* **33**, 327 (1982).
6. Y. Tomioka, S. Imazeki, N. Tanaka, *Chem. Phys. Lett.* **174**, 433 (1990).
7. M. Born and E. Wolf, *Principles of Optics* (Pergamon, New York, 1980), chap. 1, pp. 55–70.
8. P. Fromherz, *Nature* **231**, 267 (1970).
9. A. Chatterjee and S. N. Chatterjee, *J. Mol. Biol.* **11**, 432 (1965).
10. M. J. Bedzyk, G. M. Bommarito, J. S. Schildkraut, *Phys. Rev. Lett.* **62**, 1376 (1989).
11. Y. Sasaki and K. Hirokawa, *Appl. Phys. A* **50**, 397 (1990).
12. A. F. S. A. Habeeb, *Anal. Biochem.* **14**, 328 (1966).

13. The authors thank Y. Tomioka for preparing the sample, A. Fukuhara for discussion, S. Imazeki for advice about charged LB film, and K. Kina for advice about labeling protein. This study was performed under the approval of the National Laboratory for High Energy Physics (proposal no. 93-Y003).

25 August 1993; accepted 29 October 1993

New Light on the Heart of Darkness of the Solar Chromosphere

S. K. Solanki,* W. Livingston, T. Ayres

Solar carbon monoxide spectra indicate the existence of a cool (less than 4000 kelvin) component to the solar chromosphere coexisting with the hot, bright gas at 6000 to 7000 kelvin. However, both the existence and the location of the cool component have been controversial. New high-resolution spectra show that carbon monoxide goes into emission just beyond the limb, allowing it to be probed without photospheric contamination. The cool component has temperatures as low as 3000 to 3500 kelvin and appears to cover 50 to 85 percent of the quiet solar surface. There is a steep temperature rise to normal chromospheric temperatures at a height of 900 to 1100 kilometers. Large horizontal velocities are seen, suggesting that the cool component is maintained by the supersonic adiabatic expansion of upwelling gas in overshooting granules.

The chromosphere of the sun is prototypical for the chromospheres of most cool stars. Any major challenge to the understanding of its structure will accordingly reverberate through many areas of solar and stellar physics. We report here on observations that strongly support the need for a fundamental revision of the traditional picture of the chromosphere as a relatively homogeneous thermal structure, with a temperature lying between 5000 and 7000 K over most of its height (*1*). Models based on this picture reproduce an impressive array of observations, mainly atomic spectral lines and continuous spectra, but possess one major flaw. They cannot match observations of the fundamental vibration-rotation band of the CO molecule at 4 to 5 μm (*2*). On the other hand, previous models based on the CO lines (*2, 3*) cannot be easily reconciled with the traditional optical and ultraviolet diagnostics. This inconsistency has led some researchers to doubt the very existence of a cold component (*4, 5*), and there is general agreement that its key properties—particularly the horizontal and vertical extents—are highly uncertain (*6*).

The major hindrance to the removal of these inconsistencies and uncertainties, the lack of high spatial resolution infrared instrumentation, has been overcome recently with the installation of a large infrared grating on the main spectrograph of the McMath-Pierce facility on Kitt Peak, near Tucson, Arizona. Spectra at 4.67 μm were obtained in April 1993 at the solar limb under conditions of exceptionally low smearing by the Earth's atmosphere and low atmospheric water vapor (Figs. 1 and 2). Outside the continuum limb the CO spectrum is clearly in emission.

From the observed continuum limb profile we first determined the spatial smearing due to the finite telescope aperture, spectrograph slit width, atmospheric blurring, and scattered light, assuming a regular limb. The observations were best reproduced without any atmospheric blurring. Perhaps a quiescent "random walk" atmosphere prevailed (*7*). We then used the inferred smearing and scattering parameters to estimate the true limb profile of the CO line core emission (Fig. 3). The brightness temperature of the optically thick CO line cores remains constant at 3600 to 3900 K to approximately 0.4 arc sec outside the 4.7-μm continuum limb (corresponding to the

---

S. K. Solanki, Institute of Astronomy, ETH-Zentrum, CH-8092 Zürich, Switzerland.
W. Livingston, National Solar Observatory, National Optical Astronomy Observatories, Tucson, AZ 85726.
T. Ayres, Center for Astrophysics and Space Astronomy, University of Colorado, Boulder, CO 80309–0391.

*To whom correspondence should be addressed.